Triple Collocation of Summer Precipitation Retrievals from SEVIRI over Europe with Gridded Rain Gauge and Weather Radar Data

R. A. ROEBELING

Royal Netherlands Meteorological Institute (KNMI), De Bilt, Netherlands, and EUMETSAT, Darmstadt, Germany

E. L. A. WOLTERS, J. F. MEIRINK, AND H. LEIJNSE

Royal Netherlands Meteorological Institute (KNMI), De Bilt, Netherlands

(Manuscript received 26 July 2011, in final form 10 June 2012)

ABSTRACT

Quantitative information on the spatial and temporal error structures in large-scale (regional or global) precipitation datasets is essential for hydrologic and climatic studies. A powerful tool to quantify error structures in large-scale datasets is triple collocation. In this paper, triple collocation is used to determine the spatial and temporal error characteristics of three precipitation datasets over Europe—that is, the precipitation-properties visible/near infrared (PP-VNIR) retrievals from the Spinning Enhanced Visible and Infrared Imager (SEVIRI) instrument on board Meteosat Second Generation (MSG), weather radar observations from the European integrated weather radar system, and gridded rain gauge observations from the datasets of the Global Precipitation Climatology Centre (GPCC) and the European Climate Assessment and Dataset (ECA&D) project. For these datasets the spatial and temporal error characteristics are evaluated and their performance is discussed. Finally, weather radar and PP-VNIR retrievals are used to evaluate the diurnal cycles of precipitation occurrence and intensity during daylight hours for different European climate regions. The results suggest that the triple collocation method provides realistic error estimates. The spatial and temporal error structures agree with the findings of earlier studies and reveal the strengths and weaknesses of the datasets, such as inhomogeneity of weather radar practices across Europe, the effect of sampling density in the gridded rain gauge dataset, and the sensitivity to retrieval assumptions in the PP-VNIR dataset. This study can help us in developing satisfactory strategies for combining various precipitation datasets—for example, for improved monitoring of diurnal variations or for detecting temporal trends in precipitation.

1. Introduction

Accurate information on spatial and temporal variations in precipitation occurrence (areal or temporal fraction at which precipitation occurs) and intensity (rain rates) is of great importance for evaluating precipitation parameterizations in weather and climate models and for studying feedbacks between precipitation and atmospheric or surface quantities. These studies require information at high spatial and temporal resolutions. Although operational weather radars provide information on precipitation occurrence and intensity and the networks of these radars are established over Europe and the United States, large areas of the world remain undersampled or are not sampled at all (e.g., ocean). Passive imagers operated on geostationary satellites can bridge this gap and provide quasi-global information on the occurrence and intensity of precipitation.

Over the past decades, several methods have been developed to detect precipitating clouds and retrieve rain rates from passive imagers (Kidd and Levizzani 2011). The methods developed for geostationary satellites often use thermal infrared observations and relate daily minimum cloud-top temperatures (Adler and Negri 1988) or cold cloud durations (CCD) to rain rates (Todd et al. 1995). The infrared-based methods give fair accuracies over areas where rainfall is governed by deep convection. The use of visible and near-infrared observations offers the opportunity to base precipitation retrievals on cloud physical properties and improve these

Corresponding author address: R. A. Roebeling, EUMETSAT, Eumetsat Allee 1, D-64295 Darmstadt, Germany.
E-mail: rob.roebeling@eumetsat.int

DOI: 10.1175/JHM-D-11-089.1

retrievals during daylight hours. Past studies on the application of visible and near-infrared observations for the detection of precipitating clouds include Rosenfeld and Gutman (1994), Lensky and Rosenfeld (2006), Nauss and Kokhanovsky (2006), and Thies et al. (2008). Roebeling and Holleman (2009) developed a cloud-microphysics-based algorithm to retrieve precipitation occurrence and intensity named the precipitation properties visible and near infrared (PP-VNIR) algorithm. Although their algorithm only requires visible and near-infrared observations from passive imagers, it combines two physical approaches that have been developed for visible and near-infrared observations and microwave radiometer (MWR) observations, respectively.

The retrieval of precipitation intensities for stratiform and convective clouds is also feasible with the more physically based satellite MWR retrieval methods (e.g., Conner and Petty 1998; Wentz and Spencer 1998) that relate retrieved liquid water path and rain column height to precipitation intensity. The main drawbacks of the MWR-based retrievals are that they apply best to liquid precipitation and are only available from low earth-orbiting satellites, and hence have a very limited time resolution. Although various algorithms have been developed for the retrieval of solid precipitation from MWR observations, among others the Goddard profiling algorithm (GPROF) (Kummerow et al. 2001), observing this type of precipitation from space remains challenging. For example, because the observation of solid hydrometeors is hampered by solid precipitation that is already lying on the surface, it is difficult to properly discern the atmospheric precipitation signal. In addition, the intensity of solid precipitation is usually light and therefore difficult to detect. The way forward, however, is complex as it requires a multisensor approach combining active and passive instrument observations, as well as a need to increase our physical understanding of the microphysical and radiative properties of ice hydrometeors (Levizzani et al. 2011; Grecu and Olson 2008).

Beside single-instrument retrievals, methods have been developed that combine measurement from different sources. The Climate Prediction Center morphing method (CMORPH) provides global precipitation estimates by propagating motion vectors derived from geostationary satellite infrared observations on passive microwave satellite scans (Joyce et al. 2004). The Global Precipitation Climatology Project (GPCP) (Adler et al. 2003) merges measurements from different sources—that is, precipitation estimates from low-orbit satellite microwave data, geosynchronous-orbit infrared satellite data, surface gauge precipitation observations from the Global Precipitation Climatology Centre (GPCC; Rudolf et al. 2011), as well as observations from the Television and Infrared Observation Satellite (TIROS) Operational Vertical Sounder (TOVS) and the Atmospheric Infrared Sounder (AIRS) for the regions outside $\pm 40^\circ$ latitude. The Precipitation Estimation from Remotely Sensed Information using Artificial Neural Networks (PERSIANN) combines information from infrared and microwave satellite imagery and ground-surface topography to estimate precipitation for which rain gauge and weather radar data are used for calibration (Hsu et al. 1997). Examples of other retrieval methods that combine passive microwave observations and infrared observations from geostationary satellites are the Tropical Rainfall Measuring Mission (TRMM) Multisatellite Precipitation Analysis (TMPA) method (Huffman et al. 2007) and the Global Satellite Mapping of Precipitation (GSMaP) method (Aonashi et al. 2009). Because most combined precipitation products are tuned toward rain gauge observations, their bias with respect to these observations is small. However, combining information from different sources with different temporal and spatial resolutions will change the statistics of the precipitation datasets. Although several combined retrieval methods apply statistical histogram matching to reconstruct the original precipitation statistics (e.g., Adler et al. 2003; Huffman et al. 2007), these methods are less suited for evaluating the probability density functions of precipitation as is done in studies of, for example, extreme statistics.

Conventional measurements of rain from gauges provide a direct physical measurement of surface precipitation. These types of measurements are subject to errors arising from the measurement conditions, such as wind effects and evaporation, and from uncertainties caused by the representativeness of these observations to the rainfall in the surrounding areas. In addition, the network of rain gauges can be too coarse to represent regional variations, for example, in sparsely sampled regions or regions with rapidly changing topography. In contrast, weather radars and geostationary satellites can provide observations of precipitation occurrence and intensity at the required spatial and temporal scales. However, weather radar observations are subject to errors due to, for example, imprecise backscatter: rain-intensity relationships, range effects, or clutter (e.g., Battan 1973; Doviak and Zrnic 1993). On the other hand, satellite retrievals are subject to systematic errors due to, for example, assumptions on below-cloud evaporation of precipitation or empirical relationships between cloud parameters and precipitation. Finally, in comparison studies part of the differences can be attributed to synchronization and collocation uncertainties, as well as to representativeness differences (Piman et al. 2007).

A key element for error assessment studies is the availability of datasets with uncorrelated errors. When this requirement is fulfilled, approaches such as the triple collocation method can be used to estimate the errors and the cross-calibration of three linearly related datasets (Stoffelen 1998). Until now, triple collocation has been mainly applied for error estimates and calibration of scatterometer winds (Stoffelen 1998; Janssen et al. 2007) and soil moisture retrievals (Scipal et al. 2008; Dorigo et al. 2010). However, triple collocation can be applied to all types of physical parameters that represent the same spatial and temporal scales and are subject to mean random errors with a Gaussian nature.

This paper aims to determine the applicability of different types of precipitation data for climate and weather model evaluation studies. First, three precipitation datasets with independent errors are evaluated with respect to their ability to capture spatial and temporal variations in mean precipitation amounts. Hereto, we use the triple collocation analysis to quantify the residual errors of the datasets from (i) the gridded rain gauge data from GPCC and/or the European Climate Assessment and Dataset (ECA&D) projects, (ii) the observations from the European weather radar network, and (iii) the precipitation retrievals from the PP-VNIR algorithm using observations from the Spinning Enhanced Visible and Infrared Imager (SEVIRI). These residual errors are determined for the spatial variations in four-month mean precipitation amounts during three summer periods over Europe, and for the temporal variations in precipitation amount during 36 dekads (10-day periods). Second, our study will analyze whether the precipitation occurrence and intensity retrievals of weather radars and the PP-VNIR algorithm reveal similar diurnal cycles during daylight hours.

The outline of this paper is as follows. In section 2, the satellite, weather radar, and rain gauge measurements, as well as retrieval methods, are presented. In section 3, the triple collocation method is explained. The results of the triple collocation analysis for the summer months of 2005, 2006, and 2007 are presented in section 4. The applicability of weather radar observations and PP-VNIR retrievals is further discussed in section 5. Finally, in section 6, a summary is given and conclusions are drawn.

2. Measurements and methods

a. Satellite observations

Meteosat Second Generation (MSG) is a series of European geostationary satellites that are operated by the European Organization for the Exploitation of Meteorological Satellites (EUMETSAT). The first MSG satellite (*Meteosat-8*) was successfully launched in August 2002, while in December 2005 the second MSG satellite (*Meteosat-9*) was launched. The MSG is a spinning-stabilized satellite that is positioned at an altitude of about 36 000 km above the equator at 3.4°W (until May 2008) for *Meteosat-8* and 0.0° for *Meteosat-9*. The SEVIRI instrument scans Europe and Africa every 15 min and operates three channels at visible and near-infrared wavelengths between 0.6 and 1.6 μm, eight channels at infrared wavelengths between 3.8 and 14 μm, and one high-resolution visible channel at 0.7 μm. The nadir spatial resolution of SEVIRI is 1×1 km^2 for the broadband high-resolution channel and 3×3 km^2 for the other channels. Over northern Europe (the Netherlands) the satellite viewing zenith angle of SEVIRI is about 60° and, as a consequence, the spatial resolution is reduced to about 4×7 km^2.

b. Satellite retrievals

The cloud physical properties (CPP) algorithm of the Satellite Application Facility on Climate Monitoring (CM-SAF) is used to retrieve cloud phase (CPH), cloud optical thickness (COT), cloud particle size (r_e), and condensed water path (CWP) from SEVIRI reflectances (Roebeling et al. 2006). COT and r_e are retrieved for cloudy pixels in an iterative manner by simultaneously comparing satellite-observed reflectances at visible (0.6 μm) and near-infrared (1.6 μm) wavelengths with look-up tables (LUTs) of reflectances calculated for water and ice clouds with given optical thicknesses, particle sizes, and surface albedos. The LUTs have been generated with the Doubling Adding Royal Netherlands Meteorological Institute (DAK) radiative transfer model (De Haan et al. 1987; Stammes 2001). The retrieval of CPH is done simultaneously with the retrieval of COT and particle size. The phase ''ice'' is assigned to pixels for which the observed 0.6- μm and 1.6-μm reflectances correspond to simulated reflectances of ice clouds, and the cloud-top temperature is less than 265 K. The remaining cloudy pixels are considered to represent water clouds (Wolters et al. 2008). The CWP is computed from the retrieved COT and particle size. The retrievals are limited to satellite and solar viewing zenith angles smaller than 72°. Várnai and Marshak (2007) found that cloud property retrievals become more sensitive to errors with increasing satellite and solar viewing zenith angles as a result of larger inaccuracies in the radiative transfer simulations, lower signal-to-noise ratio of the reflectance observations, and larger differences between one-dimensional and three-dimensional cloud reflectances. In addition, Roebeling et al. (2008) showed that the

uncertainties in COT retrievals increase with increasing visible reflectances, which saturate at high COT values.

PP-VNIR is a cloud microphysics-based algorithm for the retrieval of precipitation occurrence and intensity from passive imager observations (Roebeling and Holleman 2009). This algorithm combines two physical approaches—that is, the approach proposed by Lensky and Rosenfeld (2006) to retrieve precipitation occurrence from visible and near-infrared observations and the approach proposed by Wentz and Spencer (1998) to retrieve precipitation intensity from integrated liquid water path and height of the rain column observations from MWRs. PP-VNIR retrieves precipitation occurrence from information on CWP, CPH, and droplet effective radius using three detection criteria. First, clouds with CWP values larger than a threshold value (CWP_T) are considered potentially precipitating. Second, information on CPH is used to separate ice from water clouds. All ice clouds with CWP values larger than CWP_T are labeled precipitating. Third, information on the droplet effective radius is used to separate precipitating from nonprecipitating water clouds. All water clouds with a droplet effective radius larger than a threshold value (r_{eT}) and CWP values larger than CWP_T are labeled precipitating. Precipitation intensity (R) is retrieved from information on CWP and height of the rain column (H) using the following equation:

$$R = \frac{c}{H}\left[\frac{\mathrm{CWP} - \mathrm{CWP}_0}{\mathrm{CWP}_0}\right]^{\alpha}, \tag{1}$$

where R is given in mm h^{-1} and H is given in km, CWP_0 is the CWP offset value in g m^{-2} above which R is calculated, α is a dimensionless constant, and c is a constant (in mm h^{-1}) km that has a value of 1. The retrieved rain intensities are limited to a maximum intensity (R_{max}). Inspired by the empirical relationship between R and CTT suggested by Vicente et al. (1998), we calculate R_{max} as function of H and an offset rain intensity (R_0) with the following equation:

$$R_{\max} = R_0 + H^{1.6}. \tag{2}$$

To reduce the impact of R_{max} on our precipitation retrievals R_0 is chosen to be conveniently large and set at 2 mm h^{-1}. Here H is determined from the difference between the highest cloud-top temperature over an area of 100×100 SEVIRI pixels (CTT_{max}), which is assumed to represent a thin water cloud with a minimum rain column height (dH), and the cloud-top temperature of the observed pixel (CTT_{pix}). Assuming that the vertical decrease in temperature obeys a wet adiabatic lapse rate of 6.5 K km^{-1}, H can be derived as follows:

$$H = \frac{(\mathrm{CTT}_{\max} - \mathrm{CTT}_{\mathrm{pix}})}{6.5} + dH. \tag{3}$$

Roebeling and Holleman (2009) calibrated the PP-VNIR algorithm over the Netherlands with weather radar observations yielding the following optimum settings for CWP_T (160 g m^{-2}), r_{eT} (15 μm), CWP_0 (120 g m^{-2}), α (1.6), and dH (0.6 km). PP-VNIR retrievals have been validated over the Netherlands against weather radar observations, where these retrievals were found to have an accuracy of about 0.8 mm h^{-1} and a precision of about 1.0 mm h^{-1} (Roebeling and Holleman 2009). Wolters et al. (2011) validated the PP-VNIR algorithm over West Africa against TRMM Precipitation Radar (TRMM-PR) and Climate Prediction Center morphing method (CMORPH) observations. They found that the difference between the PP-VNIR and TRMM-PR rain rates is within $\pm 10\%$. In addition, they showed that the PP-VNIR algorithm is well suitable for monitoring the daytime diurnal cycle of precipitation in tropical areas, where daytime diurnal cycle refers to the diurnal cycle during the daylight hours at which PP-VNIR retrievals are possible, that is, at satellite and solar viewing zenith angles smaller than 72°.

c. Weather radar observations

The Network of European Meteorological Services (EUMETNET) Operational Programme for the Exchange of Weather Radar Information (OPERA) is an ongoing European program that provides a platform to exchange expertise on operational weather radar issues and to harmonize and improve the operational exchange of weather radar information between national meteorological services (e.g., Huuskonen 2006; Holleman et al. 2008; Huuskonen et al. 2010). An important achievement of OPERA is the establishment of the exchange of weather radar data through a data hub. Current work of OPERA is focused on the harmonization and quality control and improvement of radars across Europe. The radar data used in this study is a composite of the national composites of six countries: Belgium (2), France (23), Germany (16), Ireland (2), the Netherlands (2), and the United Kingdom (14). This means that the radar data used in this paper is a European composite based on a network of 59 radars distributed over Western Europe. It should be noted that this network comprises different types of radars—that is, the majority are C-band radars (with some S-band radars), most of which are Doppler radars, and some are dual polarization radars. The European composite is provided as dBZ values, which are observed every 5 min at a horizontal resolution of 4×4 km^2. More details on

the radar network used in this study can be found in Huuskonen (2006).

Note that weather radar retrievals are not without problems and are subject to numerous uncertainties, including calibration, attenuation, beam blockage, ground clutter, or variations in the relation between the radar echoes and rainfall rate (e.g., Wilson and Brandes 1979; Krajewski et al. 2010; Hazenberg et al. 2011). Weather radar observations are only quantitatively usable for the central part of the image, covering an area of about 200 km around the weather radar station. Due to the Earth's curvature, the distance over which weather radars observe the entire cloud is limited and at KNMI a maximum range of 200 km is used for quantitative precipitation estimation (Overeem et al. 2009).

Weather radars employ backscattering of radiofrequency waves (5.6 GHz for C band) to measure precipitation and other particles in the atmosphere (e.g., Battan 1973; Doviak and Zrnic 1993). The intensity of the atmospheric echoes is converted to the so-called radar reflectivity factor (Z) using the Rayleigh-scattering approximation. This approximation is valid when the radar wavelength (5 cm) is much larger than the raindrop diameters (<6 mm). Radar reflectivity factors are converted to rainfall intensities (R) using a fixed power law (Marshall et al. 1955):

$$Z = 200R^{1.6}, \tag{4}$$

with the radar reflectivity factor Z ($\text{mm}^6\ \text{m}^{-3}$) and rainfall intensity R ($\text{mm}\ \text{h}^{-1}$). Note that the above-given Marshall–Palmer Z–R relation was found to match well to midlatitudinal conditions in the Netherlands where it has been confirmed for larger rainfall intensities. (Wessels 1972).

d. GPCC and E-OBS datasets

Gauge-based gridded precipitation datasets are another source of information. For Europe the two most widely used gauge-based gridded datasets are the GPCC dataset provided by the German Weather Service (Rudolf et al. 2011) and the European Daily High-Resolution Observational Gridded Dataset (E-OBS) provided by the Royal Netherlands Meteorological Institute (Haylock et al. 2008).

The GPCC dataset is available at a regular grid of 0.5°, 1.0°, or 2.5° at a monthly resolution. This dataset covers the global land areas excluding Greenland and Antarctica over a period of more than 100 years (1901–2009), and is freely available for scientific purposes (http://gpcc.dwd.de). This gridded dataset is generated from the most comprehensive station database of monthly observed precipitation worldwide. The amount of available stations varies with time, and reached a maximum of about 45 000 stations globally in 1986/87. Over Europe the number of observing stations is larger than 7000. These stations are unevenly distributed, with the highest densities in Germany, France, the United Kingdom, the Netherlands, and Switzerland. All observations in this database are subject to a multistage quality control to minimize the risk of generating temporal inhomogeneities in the gridded data due to varying station densities. Hereafter the data are projected on a regular grid by spatially interpolating the anomalies from climatological normals at the stations using a modified version of the sphere map method (Willmott et al. 1985) and superimposing these gridded anomalies on the background climatology. For our study we used the GPCC Full Data Reanalysis Product version 4 of monthly precipitation amounts projected at regular grid of $0.5° \times 0.5°$.

The E-OBS dataset of rain gauge observations is available on a regular grid of $0.25° \times 0.25°$ at a daily resolution. The daily observations at point locations are taken from the ECA&D (http://eca.knmi.nl) comprising a set of about 2300 observing stations. These stations are unevenly distributed, with the highest densities in the United Kingdom, the Netherlands, and Switzerland. E-OBS provides land-only information on precipitation amounts and minimum, maximum, and mean surface temperatures over Europe for the period 1950–2006 (Haylock et al. 2008). This dataset improves on previous products in its spatial resolution and extent, time period, number of contributing stations, and attention to find the most appropriate method for spatial interpolation of daily climate observations. The dataset has been designed to provide the best estimate of gridbox averages rather than point values to enable direct comparisons with regional climate models. The interpolation process is employed in three steps. First, the monthly precipitation totals and monthly mean temperature are interpolated using three-dimensional thin-plate splines. Second, the daily anomalies are interpolated using indicator and universal kriging for precipitation and kriging with an external drift for temperature. Finally, the monthly and daily estimates are combined. Interpolation uncertainty is quantified by the provision of daily standard errors for every grid square.

3. Triple collocation

In this section we will introduce the general principles of the triple collocation method. Triple collocation assumes that the rainfall datasets (R_x) are related to a hypothetical true precipitation (R) as follows (Stoffelen 1998):

$$\begin{aligned} R_g &= \alpha_g + \beta_g R + e_g \\ R_r &= \alpha_r + \beta_r R + e_r \\ R_s &= \alpha_s + \beta_s R + e_s \end{aligned} \tag{5}$$

in which α_x are the offsets, β_x the gains, and e_x the residual errors. Here x represents the gridded rain gauge (g), weather radar (r), and satellite (s) datasets. To eliminate differences due to differences in the α_x and β_x, the three datasets are recalibrated to the hypothetical true precipitation R. The recalibrated datasets are defined as $R_x^* = R + e_x^*$, which are calculated by eliminating the calibration coefficients in the observational datasets $R_x^* = R_x/\beta_x - \alpha_x/\beta_x$ and in the residual errors $e_x^* = e_x/\beta_x$. Because the hypothetical true precipitation is not known, one of the three datasets is chosen as a reference. The residual errors do not depend on the chosen reference dataset. Now the unknown true precipitation can be removed, and Eq. (5) can be rewritten to

$$\begin{aligned} R_g^* - R_r^* &= e_g^* - e_r^* \\ R_g^* - R_s^* &= e_g^* - e_s^* \\ R_r^* - R_s^* &= e_r^* - e_s^*. \end{aligned} \tag{6}$$

By cross multiplying the equations of Eq. (6) and assuming that the residual errors are uncorrelated, the mean variance of residual errors $\langle e_x^{*2} \rangle$ can be fully determined by three independent and calibrated precipitation estimates using the following equations:

$$\begin{aligned} \langle e_g^{*2} \rangle &= \langle (R_g^* - R_r^*)(R_g^* - R_s^*) \rangle \\ \langle e_r^{*2} \rangle &= \langle (R_r^* - R_g^*)(R_r^* - R_s^*) \rangle \\ \langle e_s^{*2} \rangle &= \langle (R_s^* - R_g^*)(R_s^* - R_r^*) \rangle . \end{aligned} \tag{7}$$

The triple collocation errors that are evaluated in this paper are $\langle e_g^* \rangle$, $\langle e_r^* \rangle$, and $\langle e_s^* \rangle$. We assume that the datasets represent similar spatial and temporal scales and that their error structure is Gaussian. Note that, if the datasets resolve different scales, the variance common to the smaller spatial and/or temporal scales are part of the variances of residual errors. These variances, also referred to as the representativeness errors, can be minimized by rescaling all datasets to the scale of the coarsest dataset.

4. Results

In this section we present the results of the triple collocation analysis. The data used for this analysis are the daily E-OBS and the monthly GPCC gridded rain gauge datasets and the 15-min weather radar and PP-VNIR precipitation occurrence and intensity datasets. The study is performed for European land for the four summer months May–August and the years 2005, 2006, and 2007. The area restriction is imposed by the criterion of data availability in all datasets. The study period restriction is imposed by the criterion of maximum data availability over Europe, which is achieved during the summer months owing to the limitation of PP-VNIR retrievals to daylight hours (solar zenith angles $< 72°$). Moreover, the precipitation retrievals from the PP-VNIR algorithm and from the weather radar observations are less reliable over Europe during the winter season when precipitation manifests in more different forms (e.g., convective, stratiform, drizzle, and solid precipitation) than during the summer season when convective precipitation is the most dominant form. The weather radar data were used to calculate the ratios between 24-h and daytime precipitation on a pixel-by-pixel basis, which were used to convert the daytime PP-VNIR retrievals to 24-h sums. Wüest et al. (2009) found that diurnal cycles of precipitation, derived from weather radar data that are bias corrected with daily rain gauge observations, provide accurate diurnal cycles of precipitation occurrence and intensity. Their study confirms that temporal variations in weather radar data may be used to convert the daytime values to 24-h sums.

a. Justification of the triple collocation analysis

As stated in section 3, the main assumptions behind triple collocation are that all datasets are linearly related and that the errors are Gaussian (normally distributed). We tested these assumptions to justify the use of triple collocation. The gridded rain gauge, weather radar, and PP-VNIR datasets were averaged over sufficiently long periods and regridded to sufficiently low resolutions to achieve datasets that are normally distributed. It can then be assumed that the errors are normally distributed as well. Figure 1 shows, for these datasets, the frequency distributions of the mean precipitation amounts over the months May–August of 2006 at $0.25° \times 0.25°$ degrees resolution. In general, the precipitation amounts of the gridded rain gauge and PP-VNIR datasets are normally distributed, which confirms that the accumulation over four summer months is sufficiently long. Notably, the distribution of precipitation amounts from weather radar data are distributed differently and slightly skewed toward higher amounts. It is suggested that these differences are caused by inhomogeneity of radar practices across Europe. In the next subsection the regional biases among the different weather radars will be addressed in more detail. It needs to be mentioned that it is more difficult to ascertain a Gaussian nature for dekadal precipitation amounts that are used for the analysis of the temporal triple collocation errors. A dekadal precipitation

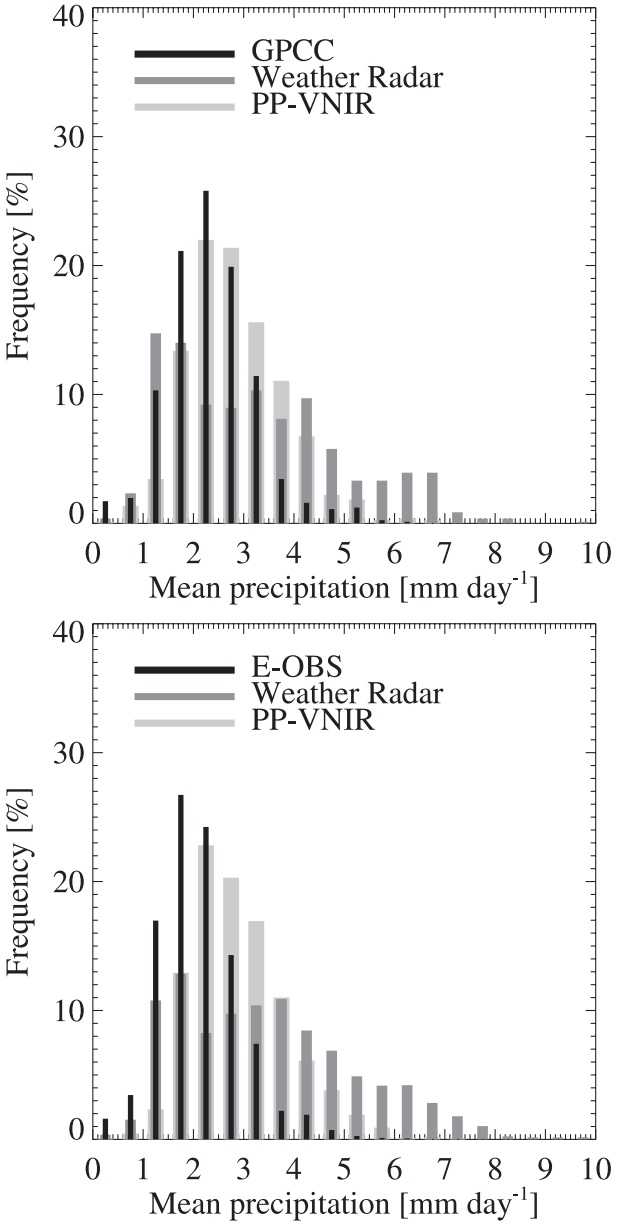

FIG. 1. Frequency distributions of (top) GPCC and (bottom) E-OBS mean precipitation amounts (mm day^{-1}) for the period May-August 2006 over Europe against those inferred from weather radar and PP-VNIR.

amount represents the mean precipitation over a 0.25 × 0.25 degree grid box aggregated over 10-day periods. Since the number of samples used to calculate a dekadal precipitation amount is considerable [about 16 800 samples per gridbox per dekad for the PP-VNIR and weather radar retrievals (10 days × 12 h × 4 obs h^{-1} × 35 obs/grid box)] the sampling period is acceptably long to obtain a Gaussian distribution. The linearity between the three datasets was verified and confirmed as well (not shown). Furthermore, Roebeling and Holleman (2009) compared precipitation occurrence and intensity retrievals from the PP-VNIR algorithm and weather radar observations data over the Netherlands. They also found that both datasets were linearly related and correlated ~0.9 for precipitation occurrence and ~0.7 for precipitation intensity. Similarly, Wolters et al. (2011) found linear relationships between rain gauge, TRMM-PR, CMORPH, and PP-VNIR datasets over West Africa.

b. *Spatial errors in the precipitation datasets*

To quantify the spatial errors in the precipitation datasets the triple collocation errors, referred to as triple errors, were calculated for the mean precipitation amounts over the months May–August, expressed in mm day^{-1}, for the years 2005, 2006, and 2007. The weather radar and PP-VNIR datasets were resampled to the spatial resolution of the datasets with the coarsest resolution, which is 0.50 × 0.50° when the GPCC dataset is used and 0.25° × 0.25° in case the E-OBS dataset is used. As an example, Fig. 2 presents the spatial distributions of the precipitation amounts over the summer months of 2006, as derived from the E-OBS, PP-VNIR, and weather radar datasets. These types of datasets (images) were generated for the summer months of 2005, 2006, and 2007. For each year of summer months a single triple error is calculated from three of these datasets, which is representative for the spatial coherence between these datasets for the entire observation domain and period of summer months. The triple errors and datasets statistics are presented in Table 1 taking E-OBS as a reference and Table 2 taking GPCC as a reference.

A qualitative analysis of this Fig. 2 reveals large differences between the three datasets. Especially, the weather radar data deviate much from the other two datasets and seem to be wetter over major parts of France and drier over major parts of the British Isles as compared to the other datasets. These regional differences are in agreement with the results of Lopez (2008) and Kidd et al. (2012), who found that the OPERA precipitation radar composite exhibits systematic and consistent differences with respect to CMORPH, rain gauge, and European Centre for Medium-Range Weather Forecasts model datasets. They found that the OPERA precipitation radar composite observes more precipitation over France and the North Sea, while a strong deficit is observed over the British Isles.

Although the spatial patterns of the E-OBS and PP-VNIR datasets are similar, the absolute precipitation amounts of E-OBS are systematically lower than the PP-VNIR amounts. This is confirmed by the statistics presented in Table 1 and Table 2. Compared to E-OBS, the median precipitation amounts of PP-VNIR and weather radar are respectively about 0.75 and 1.25 mm day^{-1}

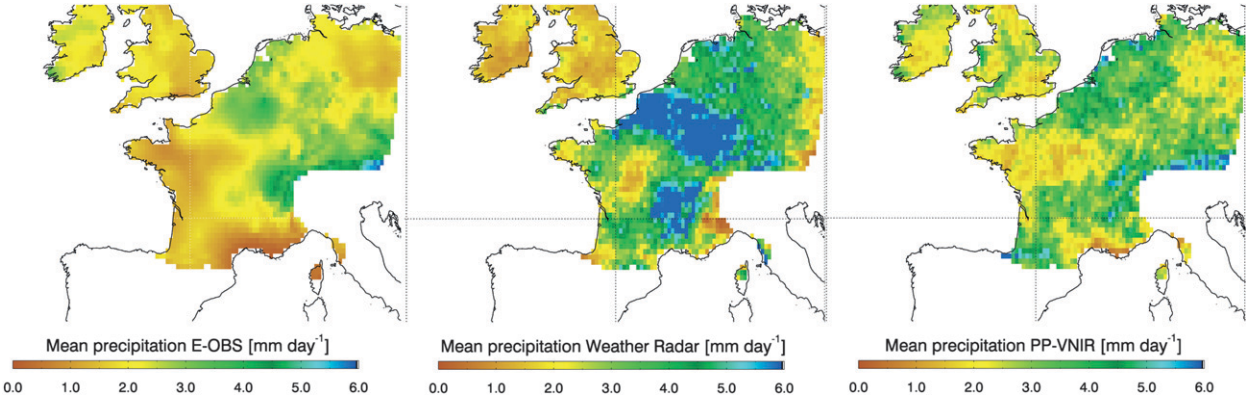

FIG. 2. Example of the mean daily precipitation amounts (mm day^{-1}) from (left) E-OBS, (center) weather radar, and (right) PP-VNIR over the period May–August 2006. All datasets are presented at the E-OBS equal latitudinal grid of 0.25° × 0.25°. Over the entire domain the mean daily precipitation amounts are 2.12 mm day^{-1} for E-OBS, 3.51 mm day^{-1} for weather radar, and 2.91 mm day^{-1} for PP-VNIR.

higher, while they are respectively about 0.45 and 1.00 mm day^{-1} higher for GPCC. It is noteworthy that there is a bias of about 0.25 mm day^{-1} between the median precipitation amounts of GPCC (Table 1) and E-OBS (Table 2). This bias may be explained by differences in quality control procedures (van den Besselaar et al. 2012), by differences in the number of observing stations, and in the interpolation method that is used to prepare the datasets (Hofstra et al. 2010). The GPCC dataset is likely to be more accurate over Germany and France where many more observing stations contributed to GPCC than to E-OBS. The correlations, which were calculated relative to the E-OBS or GPCC datasets, show that the PP-VNIR retrievals correlate fairly well with these datasets, better than 0.62 for E-OBS and better than 0.71 for GPCC, whereas the weather radar data correlate very weakly with these datasets. The triple errors of E-OBS, GPCC, and PP-VNIR are of the same order of magnitude and never exceed 1.0 mm day^{-1}. PP-VNIR consistently has smaller errors than the weather radar observations. It also has smaller errors than E-OBS and GPCC for one of the three years.

The high triple errors in the weather radar data have three reasons. First, the weather radar composite is constructed from observations of a network of 59 weather radars. Making a reliable European composite requires very good harmonization between these radars. This is difficult to achieve because the network comprises different types of radars (see section 2), operated by six different national meteorological services. It implies that there are different detection thresholds, clutter filters, and calibration procedures as well as different operational practices. This may cause differences between radars (and especially countries) in retrieved rainfall. In addition, Lopez (2008) found that part of the observed differences resulted from errors in the

TABLE 1. Statistics and triple errors for spatial variations in precipitation amounts during summer months (May – August) of 2005, 2006, and 2007 for EOBS, weather radar, and PP-VNIR. Note that the correlations (Corr) are calculated against E-OBS.

Dataset	Median (mm day^{-1})	95th % (mm day^{-1})	Std dev (mm day^{-1})	Error (mm day^{-1})	Corr (–)
		2005			
E-OBS	1.76	2.82	0.85	0.53	1.00
Weather radar	3.01	4.98	1.56	19.69	0.04
PP-VNIR	2.84	4.15	1.04	0.75	0.68
		2006			
E-OBS	2.03	3.11	0.82	0.63	1.00
Weather radar	3.30	6.09	1.81	2.16	0.34
PP-VNIR	2.77	4.22	0.96	0.82	0.62
		2007			
E-OBS	3.06	3.87	0.85	0.91	1.00
Weather radar	4.45	6.99	2.07	6.38	0.13
PP-VNIR	2.85	4.24	1.06	0.12	0.68

TABLE 2. Similar to Table 1 but for GPCC, weather radar, and PP-VNIR.

Dataset	Median (mm day^{-1})	95th % (mm day^{-1})	Std dev (mm day^{-1})	Error (mm day^{-1})	Corr (–)
		2005			
GPCC	2.08	3.11	0.87	0.59	1.00
Weather radar	3.05	4.93	1.50	11.54	0.08
PP-VNIR	2.86	3.98	0.97	0.85	0.82
		2006			
GPCC	2.34	3.33	0.85	0.62	1.00
Weather radar	3.33	6.18	1.73	2.18	0.35
PP-VNIR	2.77	4.07	0.89	0.57	0.71
		2007			
GPCC	3.31	4.34	0.90	0.51	1.00
Weather radar	4.46	6.87	1.95	4.02	0.22
PP-VNIR	2.82	4.13	1.01	0.63	0.74

postprocessing procedures that are used to prepare the data for OPERA. Currently, one of the main focuses of the OPERA program is to improve harmonization and data quality of radars across Europe (see section 2). Second, the radar signal is a function of distance from the radar and the terrain type, which can cause spatial biases in the observations. Third, the radar observations might be corrupted by clutter. Although sophisticated procedures to remove clutter have been applied by radar operators, a few missed events can still affect the maximum and standard deviation values of the weather radar products. This is confirmed by the high maximum rain amounts from weather radar presented in Table 1 and Table 2.

c. *Temporal errors in the precipitation datasets*

To quantify the temporal errors in the precipitation datasets, the triple errors were calculated per grid box using dekadal (10-day periods) precipitation amounts of the total number of 36 dekads during the months May–August of the years 2005, 2006, and 2007. The dekadal precipitation amounts from weather radar and PP-VNIR were resampled to the spatial resolution of 0.25° × 0.25° of the E-OBS dataset. Note that the statistics presented in this subsection (e.g., the correlations in Fig. 3 and the triple errors in Fig. 4) were calculated for each resampled grid box separately. These statistics represent the temporal relationship between the three datasets at a specific location only, and were calculated from 36 dekadal precipitation values of the three datasets for that grid box.

The triple collocation method only provides meaningful error estimates if the considered datasets represent the same physical quantity and are sufficiently correlated. This is verified by evaluating the correlations between the three datasets. Figure 3 presents the spatial distributions of correlations between dekadal precipitation amounts from weather radar and E-OBS, from PP-VNIR and E-OBS, and from weather radar and PP-VNIR. This figure shows that the weather radar is highly

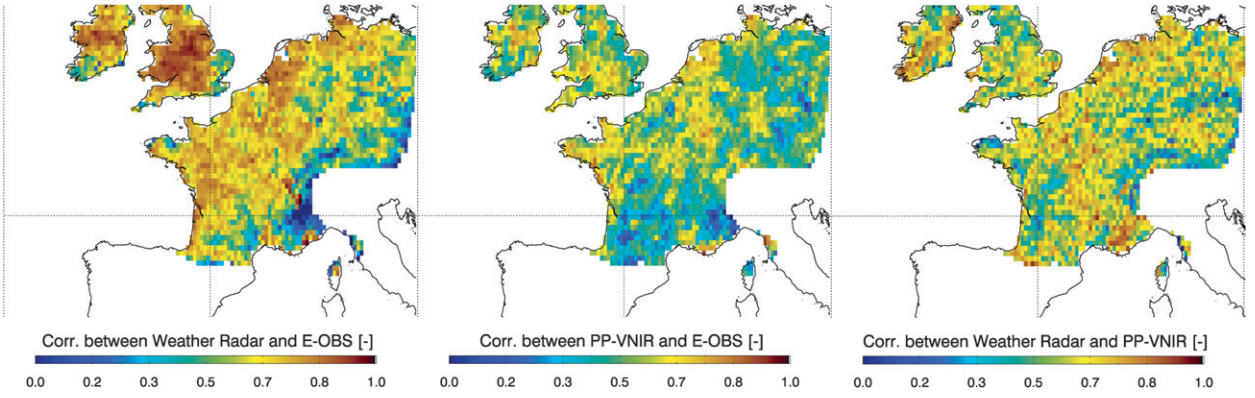

FIG. 3. Correlations between dekadal precipitation amounts from (left) weather radar and E-OBS, (center) PP-VNIR and E-OBS, and (right) weather radar and PP-VNIR for the summer months (May–August) of the years 2005, 2006, and 2007. All datasets are presented at the E-OBS equal latitudinal grid of 0.25° × 0.25°.

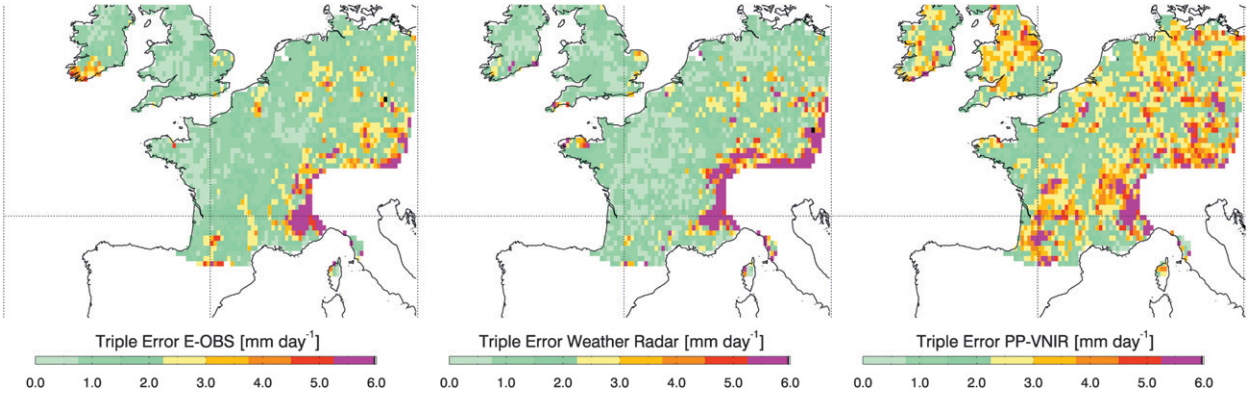

FIG. 4. Triple errors for temporal variations in dekadal precipitation amounts (mm day^{-1}) during the summer months (May–August) of 2005, 2006, and 2007 for (left) E-OBS (left panel), (center) weather radar, and (right) PP-VNIR. All datasets are presented at the E-OBS equal latitudinal grid of 0.25° × 0.25°.

correlated with the E-OBS data. The 10th and 90th percentiles of the correlations are 0.39 and 0.83. As expected, an offline evaluation of the sampling density of the rain gauges revealed that the areas with the highest correlations correspond to areas with the densest sampling, while the correlations are lower in coarser sampled and mountainous areas. The correlations between PP-VNIR and E-OBS are weaker; the 10th and 90th percentiles of the correlations are 0.34 and 0.69. These values are close to the values found for the spatial error analysis (see Table 1). The PP-VNIR correlates better with the weather radar data, with 10th and 90th percentiles of the correlations of 0.42 and 0.76.

Figure 4 presents the triple errors of the E-OBS, weather radar, and PP-VNIR datasets. This figure shows that the issues of weather radar observations regarding clutter and harmonization that greatly affect the spatial variations in precipitation amount have much less effect on temporal variations in precipitation amount on a submonthly scale. This can be seen from small triple errors in the weather radar and E-OBS datasets, which vary between 0.5 and 1.5 mm day^{-1}. The errors in the PP-VNIR dataset are higher and range between 1.0 and 2.0 mm day^{1}. These errors are close to the values that we found for the analysis of spatial errors. The strengths and weaknesses of the PP-VNIR algorithm for capturing temporal and spatial variations are similar. Given that this cannot be said for weather radar, the PP-VNIR algorithm is shown to be a valuable new source of precipitation data. This is a major advantage of using a data from a single-platform instrument (i.e., SEVIRI).

d. Evaluation of the daytime diurnal cycle

Information on the daytime diurnal cycle of precipitation occurrence and intensity is very important for model evaluations. In this subsection, the diurnal cycles of precipitation occurrence and intensity, as retrieved from weather radar and PP-VNIR observations during daylight hours, are examined in relation to prevailing atmospheric conditions. This examination is done for four subdomains, namely the Atlantic Ocean (ATL), France (FRA), Benelux (BNL), and Germany (GER). These subdomains represent different climate zones—that is, in subdomain FRA a summer convection climate with influence from the Atlantic Ocean, in subdomain BNL a maritime climate, in the subdomain GER a humid continental climate, and in subdomain ATL an oceanic climate. Figure 5 presents the location of these subdomains. In the previous subsections we have shown that the network of weather radars has great difficulty in capturing spatial variations in precipitation amounts, whereas it is well capable of capturing dekadal variations in precipitation amounts. Hence, it is more useful to normalize the daytime diurnal cycles and analyze the

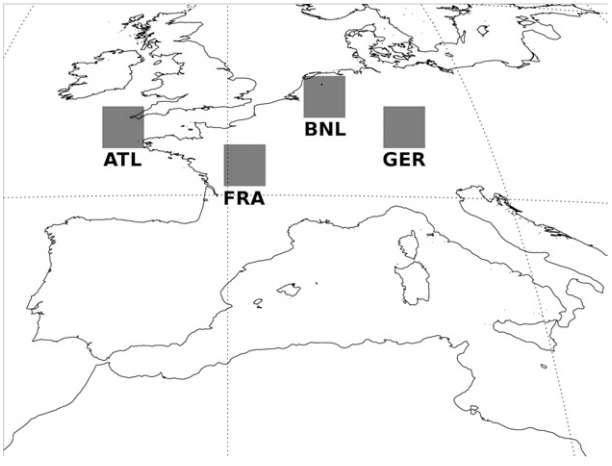

FIG. 5. Location of the subdomains: France (FRA), Benelux (BNL), Germany (GER), and the Atlantic Ocean (ATL).

standardized anomalies rather than the absolute differences. The normalized daytime diurnal cycles are calculated with the following equation:

$$\mathrm{NDP}_t = R_t / n^{-1} \sum_{t'=1}^{n} R_{t'} - 1, \tag{8}$$

where NDP is the fractional deviation from the mean (between -1 and $n - 1$), R_t is the precipitation occurrence (%) or intensity (mm h^{-1}) at time t, and n is the number of observations during the day.

Figure 6 presents the daytime diurnal cycles of normalized precipitation occurrence and intensity for the selected subdomains. The rain occurrence daytime diurnal cycles from weather radar and PP-VNIR are very similar, as can be seen from the high correlations (>0.77) and low standard deviation of the relative differences (<0.06). The daytime diurnal cycles of precipitation intensities from weather radar and PP-VNIR have lower correlations (between 0.25 and 0.87) and higher standard deviations of the relative differences (<0.26) than the precipitation occurrence cycles. It can be seen that the largest differences occur in the early morning and late afternoon. It is suggested that these differences originate from higher sensitivity of the cloud microphysical property retrievals to errors. It has been shown in several studies that cloud physical property retrievals at slant solar and/or satellite zenith angles are very sensitive to retrieval errors (Loeb and Coakley 1998; Várnai and Marshak 2007; Jonkheid et al. 2012). Especially for clouds with large optical thickness these errors can become very large (>100%). It is interesting that infrared-based retrievals also reveal a time lag in precipitation intensity at the end of the day. However, in the case of infrared-based retrievals this time lag is caused by the cirrus clouds connected to convective clouds, which can persist for some hours after a convective cloud has dissipated (Hong et al. 2006).

There are distinct differences between the daytime diurnal cycles of precipitation occurrence of the four subdomains. Over ocean (subdomain ATL) a typical stratocumulus related cycle is observed, similar to corresponding cycles over ocean surfaces found from other datasets (Negri et al. 2002; Nesbitt and Zipser 2003; Dai et al. 2007). The highest probability of rain occurs at the end of the night. During the day the stratocumulus clouds start to dissolve, which is revealed by a decreasing probability of rain as the day progresses. Over land the summertime daytime diurnal cycles of the precipitation properties are dominated by convective clouds that strongly respond to the daytime diurnal cycle of the land surface temperature. During the night, the land surface cools down and convective cloud systems collapse. During the day, the surface heats up and convective processes start to develop. The strongest convection is typically found in the afternoon when surface temperatures are highest. The daytime diurnal cycles of precipitation occurrence over the three terrestrial subdomains show remarkably similar patterns with about 20% lower (higher) occurrences during the morning (afternoon). These variations are in line with the findings of Levizzani et al. (2010), who found from infrared observations that the percentage of cold clouds over the European continent increases by about 50% from 0800 to 1600 UTC. The daytime diurnal cycles of precipitation intensity over these subdomains exhibit a pronounced peak in intensity in the afternoon. Compared to the morning, the afternoon intensities are about 70% higher over subdomain GER and about 50% higher over subdomains BNL and FRA, according to the radar data. The sharp increase in precipitation intensity over continental Europe (subdomain GER) suggests that the summertime weather over this subdomain is dominated by convection.

5. Summary and conclusions

In this paper the triple collocation method is applied to estimate spatial and temporal triple errors in three precipitation datasets, that is, gridded rain gauge (E-OBS and GPCC), weather radar, and PP-VNIR precipitation datasets. The large number of coinciding observations in these three datasets allows for a statistical assessment of the accuracy and precision of these types of information over Europe. The potential of using the PP-VNIR algorithm for precipitation occurrence and intensity retrievals from SEVIRI is shown. It is discussed that the weather radar composites face a number of shortcomings related to clutter and harmonization of the radar network with respect to obtaining spatially consistent distributions of precipitation amounts, whereas weather radar observations appear very well suited for monitoring temporal variations in precipitation.

The results show that the spatial triple errors are smaller than 1.0 mm day^{-1} for the gridded rain gauge and PP-VNIR datasets. However, the spatial triple errors in the European weather radar composite are very large (up to 18 mm day^{-1}) and the correlation to the other datasets is close to zero. It is argued that techniques to composite weather radar observations need major improvements, for example, by harmonizing algorithms, intercalibrating instruments, and improving distance correction procedures, before a spatially consistent European composite of precipitation amount can be generated from weather radar. In contrast, the analysis of temporal triple errors reveals that weather radars are capable of capturing temporal variations. Apart

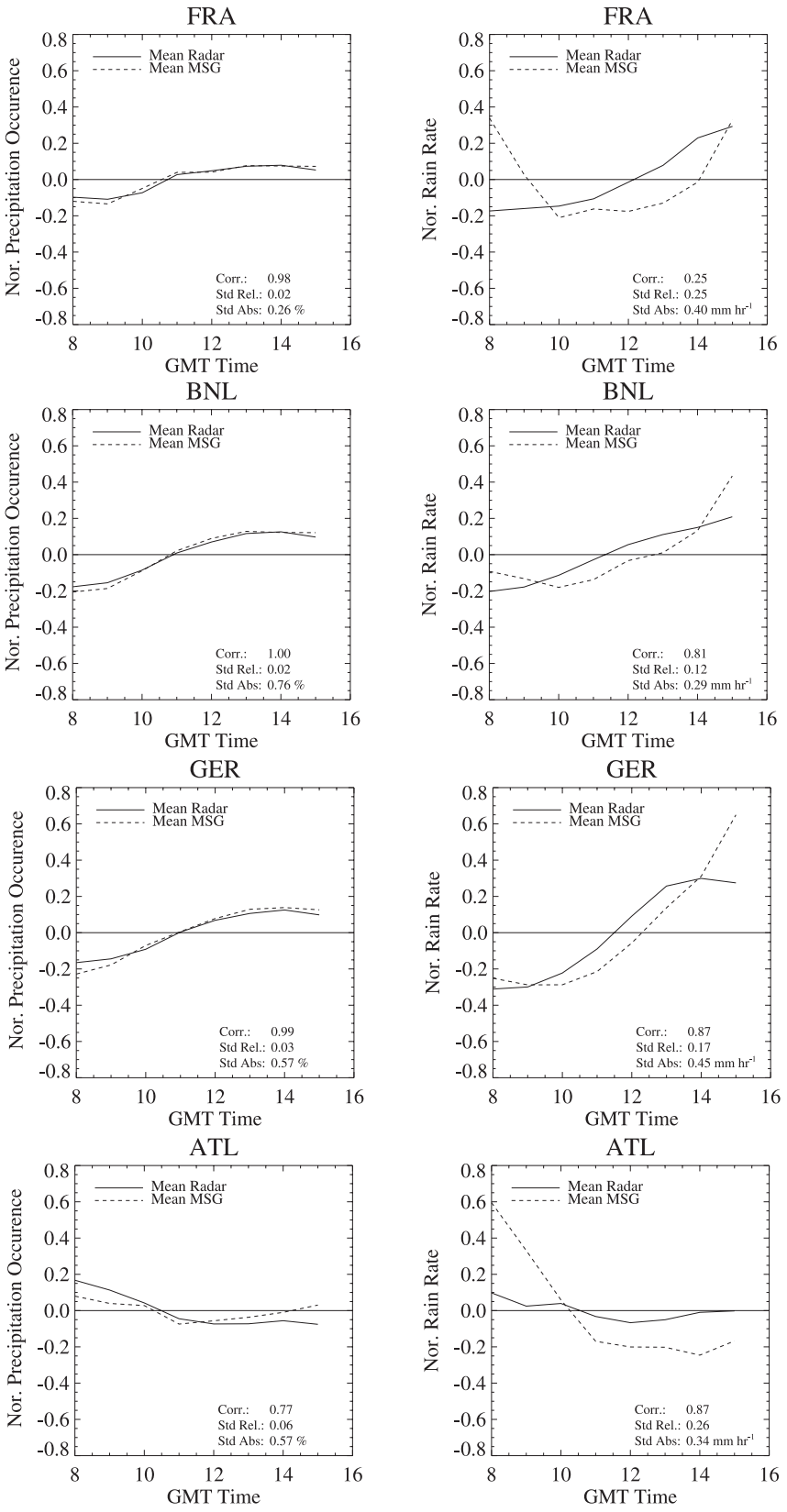

FIG. 6. Normalized daytime diurnal cycles of (left) precipitation occurrence and (right) intensity for the Benelux (BNL), France (FRA), Germany (GER), and the Atlantic Ocean (ATL) subdomains, calculated over the period May–August 2005, 2006, and 2007.

from the mountainous areas, the temporal triple errors are smaller than 1.0 mm day^{-1}.

It is shown that the daytime diurnal cycles of the precipitation occurrence retrievals from weather radar and PP-VNIR agree very well over European climate regions, with correlations between 0.8 and 1.0. Although the correlations of these cycles are lower for precipitation intensity, they still range between 0.3 and 0.9, which is reasonable. It is argued that these differences are related to the fact that the SEVIRI retrievals experience saturation for very thick clouds or during the unfavorable viewing conditions that occur during early morning or late afternoon. A disadvantage of the PP-VNIR algorithm is that the retrievals can only be carried out during daylight hours. However, PP-VNIR retrievals can be made from observations of geostationary satellites, such as MSG, at an unprecedented sampling rate of 15 min for one-fifth of the globe over land and ocean surfaces. This makes these retrievals a valuable source of information for water and energy balance studies.

This paper has shown that the triple collocation technique is a promising method to estimate the errors in precipitation datasets. The magnitudes of the spatial and temporal triple errors are reasonable and can be explained by performance issues of each dataset. The observed differences in the spatial triple errors reveal serious issues related to the aggregation of weather radar observations. This confirms the need for harmonization and quality control and improvement of radar data across Europe, which is currently one of the main focuses of the OPERA program. The observed patterns in the temporal triple errors reveal larger triple errors in the undersampled regions of the E-OBS datasets as well as in mountainous areas. Moreover, these errors show the lower ability of PP-VNIR relative to E-OBS and weather radar to monitor temporal variations in precipitation. Although triple collocation is a powerful method, it should be realized that this approach cannot be applied blindly. Two assumptions are central for the validity of the derived error model. Firstly, the residual errors need to be uncorrelated. Secondly, there need to be linear relations between the datasets. The first assumption is true because the three datasets used in this study are derived with fundamentally different observation techniques and retrieval methods. However, systematic spatial correlations may occur due to different regional uncertainties in the datasets. The second assumption is not necessarily true. Although the three datasets represent the same physical quantity, their measurement methods observe precipitation at different altitudes and sampling resolutions. Because of the latter differences, a more sophisticated calibration approach might be necessary to minimize systematic errors.

In the future, the improvement of precipitation predictions in hydrostatic and nonhydrostatic NWP models would be a very valuable step toward better forecasting of extreme weather events such as the area, intensity, and lifetime of severe rainstorms. Until recently, only weather radars could provide the frequent precipitation observations required to evaluate precipitation predictions. Upcoming radars on the European Space Agency (ESA) Earth Clouds, Aerosols, and Radiation Explorer (EarthCARE) and the 3-hourly observations that will be provided by the Global Precipitation Measurement (GPM)-era constellation of satellites are important steps toward more frequent availability of accurate precipitation data (Kidd et al. 2010) through an improved understanding of the microphysical properties of the hydrometeors and of the vertical cloud and rain column (e.g., Barker et al. 2011; Iguchi et al. 2010). However, the single-sensor PP-VNIR algorithm is unique because it combines the strong points of different methods that were developed for different satellite instruments (passive microwave and passive imagers), and it provides precipitation retrievals over land and ocean at a 15-min time resolution without the necessity of using additional information. Because the PP-VNIR retrievals are not corrected with other observations, the original precipitation statistics are conserved. Provided these statistics are realistic, they would be of great value for model evaluation studies, while datasets such as CMORPH and GPCP are less suitable for such studies.

Acknowledgments. This work was part of the Water Cycle Multi-mission Observation Strategy (WACMOS) project cosponsored by ESA and the European Reanalysis and Observations for Monitoring (EURO4M) project cosponsored by the European Union. We thank Else van den Besselaar and Wouter Greuell for their comments on earlier version of this manuscript. Further, we want to thank Wouter Dorigo for providing the triple collocation code and Ad Stoffelen for taking the time to explaining the triple collocation technique in more detail. Finally, we acknowledge the OPERA program, and in particular Iwan Holleman, for providing the European weather radar data.

REFERENCES

Adler, R. F., and A. J. Negri, 1988: A satellite IR technique to estimate tropical convective and stratiform rainfall. *J. Appl. Meteor.,* **27,** 30–51.

——, and Coauthors, 2003: The Version-2 Global Precipitation Climatology Project (GPCP) Monthly Precipitation Analysis (1979–present). *J. Hydrometeor.,* **4,** 1147–1167.

Aonashi, K., and Coauthors, 2009: GSMaP passive, microwave precipitation retrieval algorithm: Algorithm description and validation. *J. Meteor. Soc. Japan,* **87A,** 119–136.

Barker, H. W., M. P. Jerg, T. Wehr, S. Kato, D. P. Donovan, and R. J. Hogan, 2011: A 3D cloud-construction algorithm for the EarthCARE satellite mission. *Quart. J. Roy. Meteor. Soc.,* **137,** 1042–1058.

Battan, L. J., 1973: *Radar Observations of the Atmosphere*. University of Chicago Press, 324 pp.

Conner, M. D., and G. W. Petty, 1998: Validation and intercomparison of SSM/I rain-rate retrieval methods over the continental United States. *J. Appl. Meteor.,* **37,** 679–700.

Dai, A., X. Lin, and K.-L. Hsu, 2007: The frequency, intensity, and diurnal cycle of precipitation in surface and satellite observations over low- and mid-latitudes. *Climate Dyn.,* **29,** 727–744, doi:10.1007/s00382-007-0260-y.

De Haan, J. F., P. Bosma, and J. W. Hovenier, 1987: The adding method for multiple scattering calculations of polarized light. *Astron. Astrophys.,* **183,** 371–391.

Dorigo, W. A., K. Scipal, R. M. Parinussa, Y. Y. Liu, W. Wagner, R. A. M. de Jeu, and V. Naeimi, 2010: Error characterisation of global active and passive microwave soil moisture datasets. *Hydrol. Earth Syst. Sci.,* **14,** 2605–2616, doi:10.5194/hess-14-2605-2010.

Doviak, R. J., and D. S. Zrnic, 1993: *Doppler Radar and Weather Observations.* 2nd ed. Academic Press, 562 pp.

Grecu, M., and W. S. Olson, 2008: Precipitating snow retrievals from combined airborne cloud radar and millimeter-wave radiometer observations. *J. Appl. Meteor. Climatol.,* **47,** 1634–1650.

Haylock, M. R., N. Hofstra, A. M. G. Klein Tank, E. J. Klok, P. D. Jones, and M. New, 2008: A European daily high-resolution gridded dataset of surface temperature and precipitation. *J. Geophys. Res.,* **113,** D20119, doi:10.1029/2008JD010201.

Hazenberg, P., H. Leijnse, and R. Uijlenhoet, 2011: Radar rainfall estimation of stratiform winter precipitation in the Belgian Ardennes. *Water Resour. Res.,* **47,** W02507, doi:10.1029/2010WR009068.

Hofstra, N., M. New, and C. McSweeney, 2010: The influence of interpolation and station network density on the distributions and trends of climate variables in gridded daily data. *Climate Dyn.,* **35,** 841–858, doi:10.1007/s00382-009-0698-1.

Holleman, I., L. Delobbe, and A. Zgonc, 2008: Update on the European weather radar network (OPERA). *Proc. Fourth European Conf. on Radar in Meteorology and Hydrology,* Helsinki, Finland, ERAD, 3.3.

Hong, G., G. Heygster, and C. A. M. Rodriguez, 2006: Effect of cirrus clouds on the diurnal cycle of tropical deep convective clouds. *J. Geophys. Res.,* **111,** D06209, doi:10.1029/2005JD006208.

Hsu, K., X. Gao, S. Sorooshian, and H. V. Gupta, 1997: Precipitation estimation from remotely sensed information using artificial neural networks. *J. Appl. Meteor.,* **36,** 1176–1190.

Huffman, G. J., and Coauthors, 2007: The TRMM Multisatellite Precipitation Analysis (TMPA): Quasi-global, multiyear, combined-sensor precipitation estimates at fine scales. *J. Hydrometeor.,* **8,** 38–55.

Huuskonen, A., 2006: EUMETNET OPERA: Operational programme for the exchange of weather radar information. *Proc. Fourth European Conf. on Radar in Meteorology and Hydrology,* Barcelona, Spain, ERAD, 371–373.

——, L. Delobbe, and B. Urban, 2010: News on the European weather radar network (OPERA). *Proc. Sixth European Conf. on Radar in Meteorology and Hydrology,* Sibiu, Romania, ERAD, P13.2.

Iguchi, T., S. Seto, R. Meneghini, N. Yoshida, J. Awaka, and T. Kubota, 2010: GPM/DPR level-2 algorithm theoretical basis document. NASA-GSFC, 72 pp.

Janssen, P. A. E. M., S. Abdalla, H. Hersbach, and J. R. Bidlot, 2007: Error estimation of buoy, satellite, and model wave height data. *J. Atmos. Oceanic Technol.,* **24,** 1665–1677.

Jonkheid, B. D., R. A. Roebeling, and E. van Meijgaard, 2012: Quantifying uncertainties of cloud physical properties derived from simulated SEVIRI observations. *Atmos. Chem. Phys. Discuss.,* **12,** 4311–4340.

Joyce, R. J., J. E. Janowiak, P. A. Arkin, and P. Xie, 2004: CMORPH: A method that produces global precipitation estimates from passive microwave and infrared data at high spatial and temporal resolution. *J. Hydrometeor.,* **5,** 487–503.

Kidd, C., and V. Levizzani, 2011: Status of satellite precipitation retrievals. *Hydrol. Earth Syst. Sci.,* **15,** 1109–1116.

——, R. Ferraro, and V. Levizzani, 2010: The Fourth International Precipitation Working Group Workshop. *Bull. Amer. Meteor. Soc.,* **91,** 1095–1099.

——, P. Bauer, J. Turk, G. J. Huffman, R. Joyce, K.-L. Hsu, and D. Braithwaite, 2012: Intercomparison of high-resolution precipitation products over northwest Europe. *J. Hydrometeor.,* **13,** 67–83.

Krajewski, W. F., G. Villarini, and J. A. Smith, 2010: Radar-rainfall uncertainties: Where are we after thirty years of effort? *Bull. Amer. Meteor. Soc.,* **91,** 87–94.

Kummerow, C., and Coauthors, 2001: Evolution of the Goddard profiling algorithm (GPROF) for rainfall estimation from passive microwave sensors. *J. Appl. Meteor.,* **40,** 1801–1820.

Lensky, I. M., and D. Rosenfeld, 2006: The time-space exchangeability of satellite retrieved relations between cloud top temperature and particle effective radius. *Atmos. Chem. Phys.,* **6,** 2887–2894.

Levizzani, V., F. Pinelli, M. Pasqui, S. Melani, A. G. Laing, and R. E. Carbone, 2010: A 10-year climatology of warm-season cloud patterns over Europe and the Mediterranean from Meteosat IR observations. *Atmos. Res.,* **97,** 555–576, doi:10.1016/j.atmosres.2010.05.014.

——, S. Laviola, and E. Cattani, 2011: Detection and measurement of snowfall from space. *Remote Sens.,* **3,** 145–166.

Loeb, N. G., and J. A. Coakley Jr., 1998: Inference of marine stratus cloud optical depth from satellite measurements: Does 1D theory apply? *J. Climate,* **11,** 215–233.

Lopez, P., 2008: Comparison of OPERA precipitation radar composites to CMORPH, SYNOP and ECMWF model data. ECMWF Tech. Memo. 569, 22 pp.

Marshall, J. S., W. Hitschfeld, and K. L. S. Gunn, 1955: Advances in radar weather. *Advances in Geophysics,* Vol. 2, Academic Press, 1–56.

Nauss, T., and A. A. Kokhanovsky, 2006: Discriminating raining from non-raining clouds at mid-latitudes using multispectral satellite data. *Atmos. Chem. Phys.,* **6,** 5031–5036.

Negri, A. J., T. L. Bell, and L. Xu, 2002: Sampling of the diurnal cycle of precipitation using TRMM. *J. Atmos. Oceanic Technol.,* **19,** 1333–1344.

Nesbitt, S. W., and E. J. Zipser, 2003: The diurnal cycle of rainfall and convective intensity according to three years of TRMM measurements. *J. Climate,* **16,** 1456–1475.

Overeem, A., I. Holleman, and A. Buishand, 2009: Derivation of a 10-year radar-based climatology of rainfall. *J. Appl. Meteor. Climatol.,* **48,** 1448–1463.

Piman, T., M. S. Babel, A. Das Gupta, and S. Weesakul, 2007: Development of a window correlation matching method for improved radar rainfall estimation. *Hydrol. Earth Syst. Sci.,* **11,** 1361–1372.

Roebeling, R. A., and I. Holleman, 2009: SEVIRI rainfall retrieval and validation using weather radar observations. *J. Geophys. Res.,* **114,** D21202, doi:10.1029/2009JD012102.

——, A. J. Feijt, and P. Stammes, 2006: Cloud property retrievals for climate monitoring: Implications of differences between Spinning Enhanced Visible and Infrared Imager (SEVIRI) on METEOSAT-8 and Advanced Very High Resolution Radiometer (AVHRR) on NOAA-17. *J. Geophys. Res.,* **111,** D20210, doi:10.1029/2005JD006990.

——, H. M. Deneke, and A. J. Feijt, 2008: Validation of cloud liquid water path retrievals from SEVIRI using one year of CloudNET observations. *J. Appl. Meteor. Climatol.,* **47,** 206–222.

Rosenfeld, D., and G. Gutman, 1994: Retrieving microphysical properties near the tops of potential rain clouds by multispectral analysis of AVHRR data. *Atmos. Res.,* **34,** 259–283, doi:10.1016/0169-8095(94)90096-5.

Rudolf, B., A. Becker, U. Schneider, A. Meyer-Christoffer, and M. Ziese, 2011: New GPCC Full Data Reanalysis Version 5 provides high-quality gridded monthly precipitation data. *GEWEX News,* Vol. 21, No. 2, International GEWEX Project Office, Silver Spring, MD, 4–5.

Scipal, K., T. Holmes, R. de Jeu, V. Naeimi, and W. Wagner, 2008: A possible solution for the problem of estimating the error structure of global soil moisture data sets. *Geophys. Res. Lett.,* **35,** L24403, doi:10.1029/2008GL035599.

Stammes, P., 2001: Spectral radiance modeling in the UV-Visible range. *Proc. Int. Radiation Symp.,* St. Petersberg, Russia, IRS, 385–388.

Stoffelen, A., 1998: Towards the true near-surface wind speed: Error modelling and calibration using triple collocation. *J. Geophys. Res.,* **103** (C4), 7755–7766.

Thies, B., T. Nauss, and J. Bendix, 2008: Discriminating raining from non-raining clouds at mid-latitudes using Meteosat second generation daytime data. *Atmos. Chem. Phys.,* **8,** 2341–2349.

Todd, M. C., E. C. Barrett, M. J. Beaumont, and J. L. Green, 1995: Satellite identification of rain days over the upper Nile River basin using an optimum infrared rain/no-rain threshold temperature model. *J. Appl. Meteor.,* **34,** 2600–2611.

van den Besselaar, E. J. M., A. M. G. Klein Tank, G. van der Schrier, and P. D. Jones, 2012: Synoptic messages to extend climate data records. *J. Geophys. Res.,* **117,** D07101, doi:10.1029/2011JD016687.

Várnai, T., and A. Marshak, 2007: View angle dependence of cloud optical thickness retrieved by Moderate Resolution Imaging Spectroradiometer (MODIS). *J. Geophys. Res.,* **112,** D06203, doi:10.1029/2005JD006912.

Vicente, G. A., R. A. Scofield, and W. P. Menzel, 1998: The operational GOES infrared rainfall estimation technique. *Bull. Amer. Meteor. Soc.,* **79,** 1883–1898.

Wentz, F. J., and R. W. Spencer, 1998: SSM/I rain retrievals within a unified all-weather ocean algorithm. *J. Atmos. Sci.,* **55,** 1613–1627.

Wessels, H. R. A., 1972: Measurements of raindrops in De Bilt (in Dutch). KNMI Tech. Rep. WR-72-6, 41 pp.

Willmott, C. J., C. M. Rowe, and W. D. Philpot, 1985: Small-scale climate maps: A sensitivity analysis of some common assumptions associated with grid-point interpolation and contouring. *Amer. Cartographer,* **12,** 5–16.

Wilson, J. W., and E. A. Brandes, 1979: Radar measurement of rainfall—A summary. *Bull. Amer. Meteor. Soc.,* **60,** 1048–1058.

Wolters, E. L. A., R. A. Roebeling, and A. J. Feijt, 2008: Evaluation of cloud phase retrieval methods for SEVIRI on *Meteosat-8* using ground-based lidar and cloud radar data. *J. Appl. Meteor. Climatol.,* **47,** 1723–1738.

——, B. J. J. M. van den Hurk, and R. A. Roebeling, 2011: Evaluation of rainfall retrievals from SEVIRI reflectances over West Africa using TRMM-PR and CMORPH. *Hydrol. Earth Syst. Sci.,* **15,** 437–451, doi:10.5194/hess-15-437-2011.

Wüest, M., C. Frei, A. Altenhoff, M. Hagen, M. Litschi, and C. Schär, 2009: A gridded hourly precipitation dataset for Switzerland using rain-gauge analysis and radar-based disaggregation. *Int. J. Climatol.,* **30,** 1764–1775, doi:10.1002/joc.2025.